GA–A27398

# COMPARISON OF DEUTERIUM TOROIDAL AND POLOIDAL ROTATION TO NEOCLASSICAL THEORY

by
B.A. GRIERSON, K.H. BURRELL
and W.M. SOLOMON

OCTOBER 2012

GENERAL ATOMICS

GA–A27398

# COMPARISON OF DEUTERIUM TOROIDAL AND POLOIDAL ROTATION TO NEOCLASSICAL THEORY

by
B.A. GRIERSON,* K.H. BURRELL
and W.M. SOLOMON*

This is a preprint of a paper to be presented at the 24th IAEA Fusion Energy Conference, October 8–13, 2012 in San Diego, California and to be published in Proceedings.

*Princeton Plasmas Physics Laboratory, Princeton, New Jersey, USA

Work supported by
the U.S. Department of Energy
under DE-FC02-04ER54698
and DE-AC02-09CH11466

GENERAL ATOMICS PROJECT 30200
OCTOBER 2012

GENERAL ATOMICS

## ABSTRACT

$D_\alpha$ emission from neutral beam heated tokamak discharges in DIII-D [J. L. Luxon, Nucl. Fusion **42**, 614 (2002)] is evaluated to deduce the local deuterium toroidal rotation for comparison to neoclassical theory. By invoking the radial force balance relation the deuterium poloidal rotation can be inferred. It is found that the deuterium poloidal flow exceeds the neoclassical value in plasmas with collisionality $\nu_i^* < 0.1$, with a stronger dependence on collisionality than neoclassical theory predicts.

## 1. INTRODUCTION

The radial electric field in a tokamak plasma, and associated $\mathbf{E}\times\mathbf{B}$ shear, provides stabilization of long wavelength turbulent modes and improves plasma confinement.[1,2] Through the radial force balance relation, the radial electric field is a combination of three terms, with dependencies on the pressure gradient, toroidal rotation and poloidal rotation $E_r = \nabla P/Zen_i + V_\varphi B_\theta - V_\theta B_\varphi$. In discharges heated by uni-directional neutral beams, the high toroidal rotation produces a large radial electric field and $\mathbf{E}\times\mathbf{B}$ flow shear that suppresses turbulent transport.[1] As toroidal rotation is lowered, the benefit of this shearing rate decreases.[3] Predictions of ITER with TGLF[4] indicate a significant increase in fusion performance with $\mathbf{E}\times\mathbf{B}$ shear, however in devices with low relative torque the benefits of the large toroidal rotation may be absent. The core $E_r$ will be determined by the contributions from the pressure gradient, toroidal rotation and poloidal flow, all having similar magnitude.[5] Although the poloidal flow is generally considered small, $V_\theta$ enters into the radial electric field multiplied by the large $B_\varphi$. Predictions of $E_r$ and plasma performance in future devices rely on calculations and simulations of the main-ion properties ($V_\varphi, V_\theta, \nabla P_i$ and $E_r$ derived from these values),[5] hence an understanding of the main-ion toroidal and poloidal flows is required when evaluating $E_r$. For ITER design parameters ($I_p$, $B_t$, NBI all clockwise from above), the contributions to $E_r$ from NBI-driven toroidal rotation and ion-diamagnetic poloidal rotation add in a positive sense ($E_r^{V_\varphi}, E_r^{V_\theta} > 0$), while the pressure gradient opposes these terms ($E_r^{\nabla P} < 0$). Therefore both large toroidal and poloidal rotation will increase the core radial electric field, and its shear.

This article investigates the toroidal and poloidal contributions to $E_r$ under low rotation conditions in DIII-D. Plasmas are either ohmic or H-mode heated with electron cyclotron heating (ECH), with short NBI pulses used for diagnostic purposes. Thus the regime considered here is well represented by $T_e \approx T_i$ and $n_b \ll n_e, n_D$, where $n_b$ is beam ion density and $n_e, n_D$ are electron and deuterium density, respectively. Main-ion[6,7] and impurity[8–10] charge exchange recombination (CER) spectroscopy are used to measure the toroidal rotation of the deuterium and carbon ions, as well as the impurity poloidal flow velocity.[11,12] Neoclassical theory is used to predict the carbon and deuterium poloidal rotation and the deuterium toroidal rotation. By comparing the measured rotational velocities, and using the radial force balance relation, the main-ion poloidal rotation can be inferred and compared to the neoclassical values. This method of comparison is done by forward modeling with neoclassical codes, as well as deducing the fundamental neoclassical quantities ($V_\theta$ and coefficients depending on collisionality) through the force balance relation. The second method permits a straightforward propagation of errors in experimental profiles and gradients.

We find that the core main-ion poloidal flow exceeds standard neoclassical estimates from the NCLASS[13] model, being significantly larger in the ion diamagnetic direction. When $E_r$ is evaluated with the main-ion constituents, we find that the poloidal rotation contribution dominates over the toroidal rotation, and the sum enhances the core radial electric field to a value larger than neoclassical estimates. A database of discharges has been evaluated, and a consistent trend has been exposed indicating a significantly larger poloidal flow at low collisionality than conventional neoclassical theories predict.

## 2. NEOCLASSICAL THEORY

Neoclassical theory provides an expected poloidal flow, given the magnetic equilibrium and plasma profiles.[14] Neoclassical poloidal flow of the main-ions is largely driven by the temperature gradient, with a coefficient $K_1$ that depends on collisionality $V_\theta = K_1 \frac{\upsilon_{Ti}\rho_i}{2L_{Ti}} \frac{BB_t}{\langle B^2 \rangle}$. Here $K_1$ is formed by evaluating the impurity concentration and parallel viscous matrix elements. Calculations of the coefficient $K_1$ can be done analytically,[14] numerically,[13,15] or determined from plasma simulations.[16–18]

In the infinite aspect ratio ($\epsilon \to 0$), pure plasma collisionless limit, the coefficient $K_1 \to 1.17$. This banana limit corresponds to main-ion poloidal flow in the ion diamagnetic direction. For higher collisionality plateau ($\nu_i^* > 1$) and Pfirsch-Schlüter ($\nu_i^* > \epsilon^{-3/2}$) regimes the coefficient changes sign and magnitude to -0.5 and -1.0 respectively. For intermediate aspect ratios $K_1$ decreases in magnitude but remains positive in the banana regime. Impurity poloidal flow is generally smaller than the main-ion flow, but is more commonly measured.[12,19–22] Impurity poloidal flow can be expressed as $V_\theta^{imp} = (\upsilon_{Ti}\rho_i/2)[(K_1 + 3K_2/)L_{Ti}^1 - L_{Pi}^{-1} + (Z_i/Z_{imp})L_{Pimp}^{-1}] \frac{BB_t}{\langle B \rangle^2}$, which largely depends on main-ion parameters due to the $Z_i/Z_{imp}$ dependence. Poloidal flow can be modified from this treatment by the turbulent Reynolds stress $-\nabla \cdot \mathbf{\Pi}_{r,\theta}^{RS}/\mu_{ii} \sim \langle \tilde{\upsilon}_r \tilde{\upsilon}_\theta \rangle$.[23] The turbulent contributions effectively add to the neoclassical level, $V_\theta = V_\theta^{NC} + V_\theta^{RS}$ (see revised calculations of Ref. [24] in Ref. [25]).Non-local effects can also provide a modification to the standard neoclassical values[17,26].

In this manuscript we make use of a number of neoclassical models. The first model that can be evaluated is the analytic Kim-Diamond-Groebner model (KDG).[14] The KDG model can be readily evaluated in post-processing of routine experimental profile analysis. The second model is the NCLASS model, evaluated through the FORCEBAL pre-processor.[13,27] Typical NCLASS evaluation retains the full viscosity coefficients that are valid across all collisionality regimes and aspect ratios(as was done previously in Refs. [12,27]), but can also be evaluated neglecting the high collisionality, Pfirsch-Schlüter viscosity. Neglecting the Pfirsch-Schlüter viscosity effectively increases the poloidal flow coefficient $K_1$, but decreases the differential poloidal flow between species. The third model is NEO,[15] a $\delta f$ Eulerian model that solves the drift-kinetic equation in a multi-ion species plasma. The fourth model is GTC-NEO,[17,26] a $\delta f$ particle-in-cell (PIC) code that solves the drift-kinetic equation by evolving a finite number of particles based on the Lagrangian equation. Toroidal rotation of the main-ion species is predicted by adding the pressure and poloidal rotation contributions to $E_r$, giving $V_\varphi^D = V_\varphi^C + B_\theta^{-1}(E_r^{\nabla P_C} - E_r^{\nabla P_D}) + B_\theta^{-1}(E_r^{V_\theta^C} - E_r^{V_\theta^D})$.

As will be seen in the following section, the choice of neoclassical model can have significant effects on the magnitude of the predicted poloidal rotation, varying by nearly a factor of two. Thus the evaluation of agreement or disagreement with neoclassical theory depends on which model is chosen to represent that theory.

## 3. EXPERIMENTAL METHOD

A sequence of discharges were performed in DIII-D to investigate the intrinsic rotation characteristics of the main-ions and impurities using the newly commissioned main-ion CER system.[6] The discharges were executed by Ohmic startup, with a single short beam pulse for diagnostic purposes. Plasma current and toroidal field were varied between 0.7-1.1 MA and -1.7, -2.0 T on a shot-by-shot basis. Diagnostic pulses provide core ion temperature, main-ion and carbon toroidal rotation, carbon poloidal rotation and carbon density. Second harmonic ECH (X-mode) of 0.9 MW was applied to trigger the low to high (L-H) confinement transition and enter ELM-free H-mode. During the H-mode phase, diagnostic beam pulses were applied to obtain the spectroscopic measurements at three more times. Diagnostic beam pulses were designed to impart zero net torque.

Early ohmic conditions have the lowest ion temperature ($T_i \sim 1.0$ keV) and highest collisionality, with line-averaged density approximately $\langle n_e \rangle = 3 \times 10^{19}$ m$^{-3}$. H-mode temperatures reach $T_i \sim 2.0$ keV with line-averaged density of $\langle n_e \rangle = 5.5 \times 10^{19}$ m$^{-3}$. No significant MHD or other instabilities were observed. During ECH a reversal of the $q$ profile develops for $\rho_{qmin} \approx 0.2 - 0.3$. Profiles of ion temperature in H-mode develop a steepened gradient inside of $\rho \sim 0.4$, and the carbon density in this region is reduced.

One example of the plasma conditions during the ECH H-mode is provided in Fig. 1(a-b). Here the profiles of electron, deuterium, and carbon density are displayed as a function of flux-surface label, $\rho = \sqrt{\psi_t/\pi/B_{center}}$, where $\psi_t$ is toroidal flux and $B_{center}$ is defined at the magnetic axis, normalized to the value at the boundary. In all cases, error bars on the experimental profiles are obtained from Monte-Carlo perturbations within the experimental data points. Ion temperature is obtained from CER and electron temperature is obtained from Thomson scattering and ECE. Figure 1(c) presents the measured carbon and deuterium toroidal rotation from the two spectroscopy systems. Here the values of toroidal rotation are presented as outboard-midplane measurements. The carbon toroidal rotation possesses a feature that is hollow in the same region of the plasma as the hollow carbon density profile, apparently caused by ECH. The deuterium toroidal rotation profile is slightly slower than carbon at outer locations, and faster at $\rho \approx 0.25$. Also included in Fig. 1(c) is the toroidal rotation profile of the deuterons from the NCLASS code.[13] This NCLASS analysis includes all viscosity contributions. It can be seen that the NCLASS prediction is significantly faster in the toroidal direction (direction of plasma current) than the measured deuterium rotation. This difference, $(V_\varphi^D - V_\varphi^C)$ is presented in Fig. 1(d), as well as predictions from two other neoclassical models; Kim-Diamond-Groebner, and NEO.

The neoclassical quantity required for the prediction of $V_\varphi^D$ is the difference $V_\theta^D - V_\theta^C$. Using radial force balance, we can define $\Delta V_\theta$ as

$$(V_\theta^D - V_\theta^C) = \frac{1}{B_\varphi}\left(\frac{\nabla P_D}{Z_D e n_D} - \frac{\nabla P_C}{Z_C e n_C}\right) + \frac{B_\theta}{B_\varphi}(V_\varphi^D - V_\varphi^C). \tag{1}$$

The terms on the RHS of Eq. (1) are readily evaluated from the equilibrium reconstruction and experimental measurements. The LHS of Eq. (1) is then defined as $\Delta V_\theta^{exp}$.

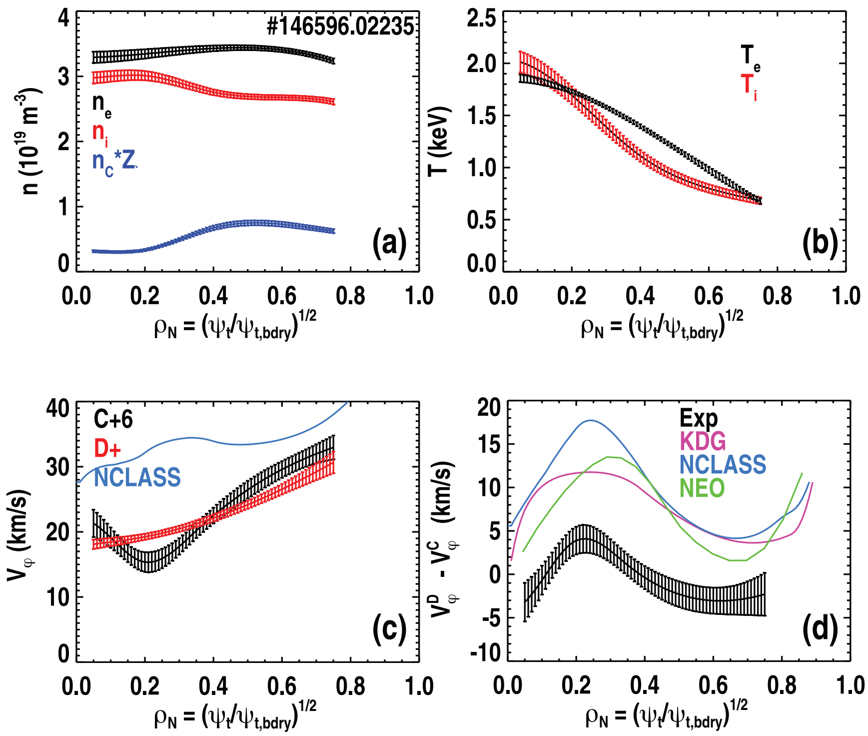


*Fig. 1. Profiles of density, temperature, toroidal rotation and differential toroidal rotation. Monte-Carlo error bars included for region where main-ion measurements are available. Differential toroidal rotation includes prediction from NCLASS and K.D.G.*

Neoclassical calculations produce $V_\theta^D$ and $V_\theta^C$ individually on the outboard midplane, and the quantity $\Delta V_\theta^{NC}$ can similarly be formed from calculations and simulations. Thus this differential poloidal flow velocity is the clearest comparison to the neoclassical theory of poloidal rotation that *does not depend on the measurement of poloidal velocity*. Comparison of $\Delta V_\theta^{exp}$ to $\Delta V_\theta^{NC}$ displays how quickly poloidally passing main ions and impurity ions move past each other. The results from experimental profiles and neoclassical theory are presented in Fig. 2(a). The experimental and neoclassical models all display the same qualitative feature, namely a peak in the differential flow velocity at the location of the largest ion temperature gradient. It is the difference between the experimental $\Delta V_\theta^{exp}$ and $\Delta V_\theta^{NC}$ that is directly manifested as a differential toroidal flow in Fig. 1(c). By examining the various models, we see that the KDG analytic model produces the smallest differential poloidal flow, followed by the NCLASS model with full viscosity evaluation, NEO and GTC-NEO. It is the NCLASS profile in Fig. 2(a) that was used to produce the toroidal rotation profile in Fig. 1(c). The fact that the NCLASS $\Delta V_\theta^{NC}$ is approximately 2 km/s below the observation is manifested as a peak 18 km/s difference in predicted toroidal flow. This is due to the factor of $B_\varphi/B_\theta$ in the equation for differential toroidal flow. The GTC-NEO model produces the largest differential poloidal flow at the location of the steep temperature gradient. Thus the conclusion from the comparison displayed in Fig. 2(a) is that the observed differential poloidal flow is within the realm of neoclassical physics for this case, even if it differs from the NCLASS model. It is noteworthy that the GTC-NEO model uses a collision operator that takes a single toroidal rotation profile, here using the more commonly measured impurity ions.

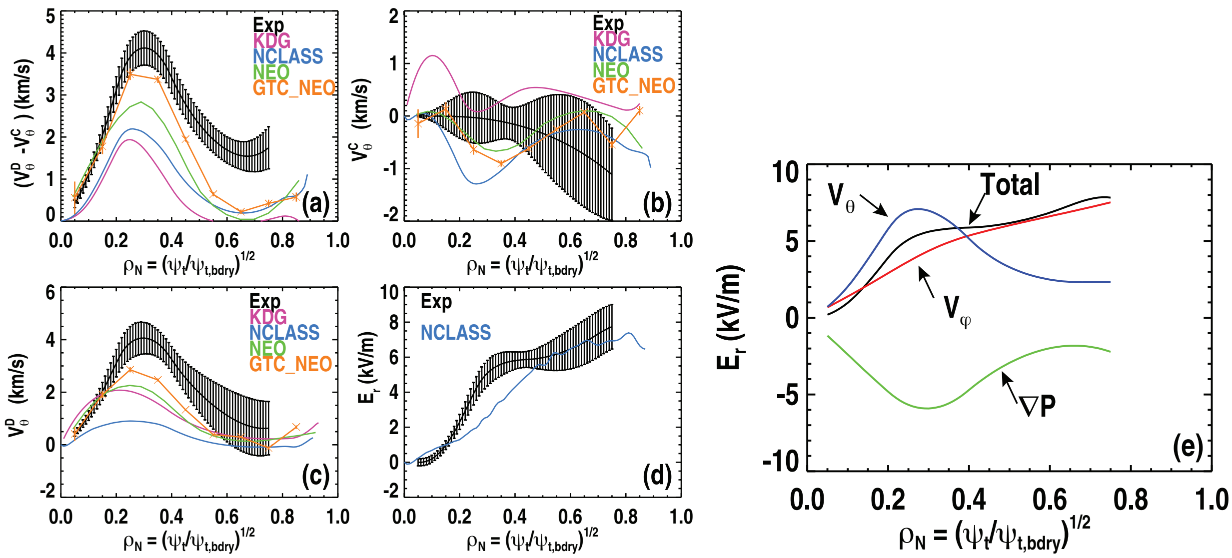


*Fig. 2. Differential poloidal rotation, carbon and deuterium $V_\theta$, and $E_r$ for the profiles in Fig. 1.*

One region of consistent disagreement between observed and measured differential poloidal flow is for $\rho > 0.5$. This disagreement calls into question the expectation of neoclassical processes dominating the experimental observations. By using the experimental profiles and performing a power balance calculation with the TRANSP[28,29] code, we can examine the ion thermal conductivity and compare to neoclassical levels. TRANP indicates that inside of $\rho \approx 0.4$ that the ion thermal conductivity $\chi_i$ is at neoclassical levels, while outside of $\rho \approx 5$, $\chi_i > \chi_i^{NC}$ by approximately a factor of ten. Thus it is likely that other cross-field transport mechanisms are dominating over neoclassical in the outer region of the plasma.

We can arrive at an inferred main-ion poloidal flow velocity by using the experimental measurements of the carbon poloidal velocity; $V_\theta^D = V_\theta^C + \Delta V_\theta$. The experimentally measured carbon poloidal flow is displayed in Fig. 2(b), along with the neoclassical calculations from the various models. As expected, the measured and predicted carbon flow velocities are small, and nearly zero within the error bars. The NCLASS model for $V_\theta^C$ displays a strong electron diamagnetic feature at $\rho \approx 0.2$, with the other two models, NEO and GTC-NEO displaying a weaker feature. However, this feature is not observed experimentally. It is noteworthy that the measured impurity poloidal flow is more ion diamagnetic than the neoclassical models in the region of steep pressure. The inferred main-ion poloidal flow is displayed in Fig. 2(c). Similar to previous investigations with impurity poloidal rotation, the inferred deuterium poloidal rotation is more ion diamagnetic than neoclassical predictions. The radial electric field is displayed in (d), (e). At the location of the steepest ion temperature gradient, the core $E_r$ is enhanced above the NCLASS estimate. By examining the contributions to $E_r$ from main-ion properties, it is clear that the poloidal rotation contribution is not negligible. Inside of $\rho$ of 0.4, the poloidal rotation dominates over the toroidal rotation term and is comparable in magnitude to the pressure gradient term.

## 4. SCALING TRENDS

In the sequence of discharges performed to investigate intrinsic rotation, the variation in plasma current naturally causes changes in plasma density, temperature and collisionality. Thus a database of measured differential poloidal flow and inferred main-ion poloidal flow can be used to expose trends in the data, and compare to expected trends in the theory. For each time in each discharge, an MSE-constrained, kinetic equilibrium reconstruction was performed using plasma profiles and ONETWO[30] transport analysis to obtain the proper $q$ profile and magnetic axis location. For each set of equilibria and profiles, the carbon poloidal rotation was determined by the method detailed in Refs. [11,12], accounting for the energy dependence and gyro-orbit cross-section effects on the apparent velocity. Each equilibrium and set of profiles were evaluated with NCLASS using full viscosity as well as neglecting Pfirsch-Schlüter viscosity (as the regime is dominantly collisionless).

The most straightforward quantity to be compared to the neoclassical theory is the measured and calculated differential poloidal flow, $\Delta V_\theta^{exp}$ and $\Delta V_\theta^{NC}$, because this quantity does not require the more complicated measure of carbon poloidal rotation. However, the differential poloidal rotation does not provide a scaling of the absolute main-ion poloidal flow, which would be beneficial to predictions of $E_r$ and $\mathbf{E}\times\mathbf{B}$ suppression of turbulence on future devices. Therefore we also form the main-ion poloidal flow by adding the measured poloidal rotation of carbon to $\Delta V_\theta^{exp}$ and computing the dimensionless poloidal flow coefficient, $K_1^{exp}$. This coefficient is also computed from the neoclassical models either directly (as in the case of KDG), or numerically by inverting the equation $V_\theta^D = (K_1/m_i\Omega_{ci})\nabla T_i$ for $K_1^{NC}$ on the outboard midplane. Here collisionality is defined as the ratio of ion-ion collision frequency to bounce frequency, $\nu_i^* = \nu_{ii}Rq/\epsilon^{3/2}v_{th,i}$. For the conditions in Fig. 1, the main-ions are in the banana collisionality regime across the entire core profile ($\nu_i^* \approx 0.05$), while carbon enters the plateau regime at $\rho \approx 0.5$. Thus we expect the main-ion poloidal flow to be ion diamagnetic, as displayed in Fig. 2(c). $K_1^{exp}(\rho)$ is consistent with expectation, being approximately 1.0 at the location of smallest collisionality. The NEO and NCLASS models are somewhat below this limit ($K_1 \approx 0.8, 0.3$, respectively), where NCLASS presents the smallest value. By neglecting Pfirsch-Schlüter viscosity in the NCLASS evaluation, the value of $K_1$ increases uniformly to $K_1 \approx 0.5$.

In order to expose scaling trends in the sequence of discharges, we evaluate the quantities $\Delta V_\theta^{exp}$, $\Delta V_\theta^{NC}$ and $K_1$ over a relatively large fixed range in $\rho = [0.2, 0.7]$ that encompasses the region exhibiting both low and high power-balance $\chi_i$, providing a general impression of the core poloidal flow properties. Figure 3(a) displays the trend in the differential poloidal flow obtained from experimental measurements, as well as differential poloidal flow from neoclassical calculations. Error bars here represent the error in $K_1$ as well as the collisionality range covered by the radial region. It is stressed that this experimental quantity does not depend on the direct measure of the impurity poloidal flow. From Fig. 3(a), we see a strong increase in the differential poloidal flow at low collisionality. This scaling trend is expected, because the strongest drive for the differential poloidal flow is the $\nabla T_i$ that naturally increases at low collisionality. The experimental $\Delta V_\theta$ exhibits a stronger scaling than the NCLASS evaluation as collisionality decreases. A simple offset would not account for the observed mismatch with the theory. Subtracting the offset would still result in a factor of two difference at $\nu_i^* \approx 0.05$.

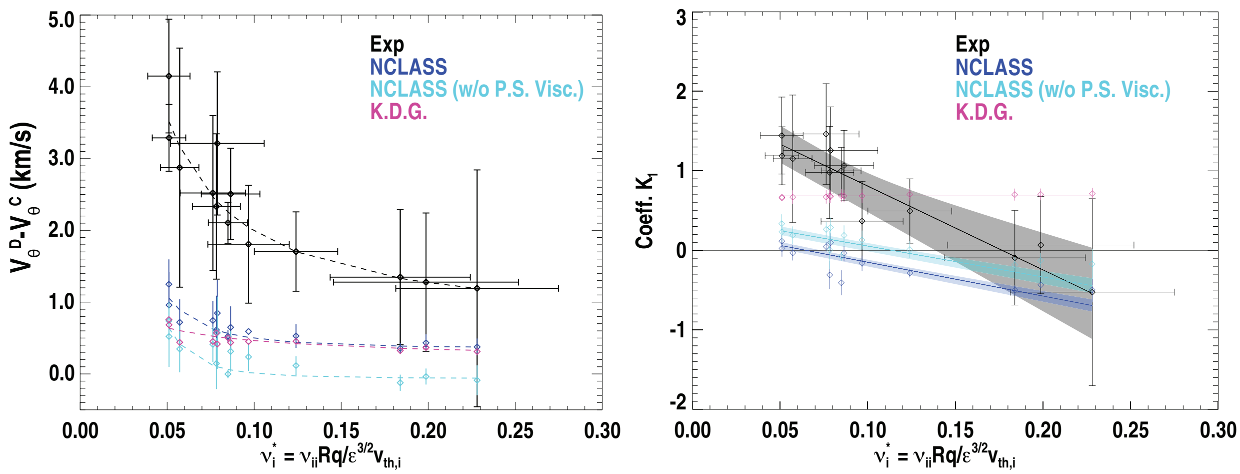


*Fig. 3. Comparison of measured differential poloidal (that does not depend on measuring either) flow to neoclassical calculations. Variation of $K_1$ with ion collisionality.*

Differential poloidal rotation has a strong dependence on the temperature gradient, and this dependence is removed by displaying the dimensionless poloidal flow coefficient $K_1$ as a function of $\nu_i^*$, presented in Fig. 3(b). An error band was formed by Monte-Carlo linear fits with error bars on both $K_1$ and $\nu_i^*$, and the shaded region falls inside of one-sigma. Scaling of $K_1$ for experimental measurements and NCLASS are approximately linear and show an increase in $K_1$ as collisionality is lowered. Experimental values are larger than NCLASS at low collisionality, and display a stronger trend. The implications are that main-ion poloidal flow is significantly more ion diamagnetic than NCLASS predictions. Neglecting the Pfirsch-Schlüter contributions to the viscosity produces a $K_1$ from NCLASS that is more positive, but not to observed levels. Scaling results from the GTC-NEO code are left to a future exercise, as the computational time is prohibitive.

The scaling trends in Fig. 3 are consistent with the reasonable agreement demonstrated in other devices at higher collisionality,[21,22] and the disagreement at lower collisionality.[12,31] Data at higher collisionality are more difficult to obtain as it requires very low ion temperatures. The inherent error bars on the measurements will dominate over the extremely low level of poloidal flow expected under those conditions, and the high collisionality regime is irrelevant to high performance plasmas.

In order to determine the effect of the anomalously high levels of poloidal flow on the core radial electric field, a simple balance of terms can be formed in the limit of zero toroidal rotation. We can compare the contributions to $E_r$ by the inequality $(B_\varphi/B)K_1\nabla T_i > T_i L_{n_i}^{-1} + \nabla T_i$. For poloidal rotation to dominate over the pressure term, this inequality must be satisfied. Given the values of $L_{n_i}^{-1} \approx 0.6$, $B \approx B_\varphi$, mid-radius $T_i \approx 15$ keV, $K_1 \approx 1$ and

$\nabla T_i \approx 15$ kV/m, then the pressure term will dominate over the poloidal rotation term by approximately 9 kV/m, giving an $E_r$ that counter-acts the toroidal rotation contribution. If, however, $K_1 \approx 2$, then the poloidal rotation dominates by approximately 1 kV/m, and adds to the core $E_r$. If $\chi_\varphi \approx \chi_i$ and $E_r^{V_\varphi} \approx 30$ kV/m,[5] then the balance of pressure and poloidal $E_r$ is significant.

## 5. CONCLUSION

A series of discharges were executed with the aim to determine the intrinsic rotation properties on main-ions and impurity ions in the DIII-D tokamak. Measurements of the toroidal rotation of main-ions and impurity ions were taken to compare to neoclassical calculations. By using the force balance relation, we find that the differential poloidal flow of carbon and deuterium ions must be significantly larger than the prediction from the NCLASS model. Other models, such as NEO and GTC-NEO are closer to experimental observations, especially in regions of the plasma where the ion thermal diffusivity $\chi_i$ is close to neoclassical levels. By using the measured carbon poloidal rotation, the main-ion poloidal rotation can be inferred and compared to neoclassical theory. We find that the deuterium poloidal flow exceeds neoclassical estimates, being more ion-diamagnetic. A database of discharges with various levels of $I_p$ and $B_t$ was constructed, and a trend of anomalous poloidal rotation at low collisionality has been observed. The construction of $E_r$ from main-ion contributions reveals that in the core of low rotation plasmas, $E_r$ can be dominated by the poloidal rotation contribution.

## REFERENCES

[1]BURRELL, K.H., Phys. Plasmas **4**, 1499 (1997).

[2]MOYER, R., et al., Phys. Plasmas **2**, 2397 (1995).

[3]POLITZER, P., et al., Nucl. Fusion **48**, 075001 (2008).

[4]KINSEY, J., et al., Nuclear Fusion **51**, 083001 (2011)

[5]BUDNY, R., et al., Nucl. Fusion **48**, 075005 (2008).

[6]GRIERSON, B.A., et al., Rev. Sci. Instrum. **83**, 10D529 (2012).

[7]GRIERSON, B.A., et al., Phys. Plasmas **19**, 056107 (2012).

[8]SERAYDARIAN, R., et al., Rev. Sci. Instrum. **57**, 155 (1986).

[9]GOHIL, P., et al., Rev. Sci. Instrum. **61**, 2949 (1990).

[10]THOMAS, D.M., et al., Fus. Sci. and Technology **53**, 487 (2008).

[11]SOLOMON, W.M., et al., Rev. Sci. Instrum. **75**, 3481 (2004).

[12]SOLOMON, W.M., et al., Phys. Plasmas **13**, 056116 (2006).

[13]HOULBERG, W.H., et al., Phys. Plasmas **4**, 3230 (1997).

[14]KIM, Y., et al., Physics of Fluids B: Plasma Physics **3**, 2050 (1991).

[15]BELLI, E. and CANDY, J., Plasma Physics **50**, 095010 (2008).

[16]DIF-PRADALIER, G., Phys. Plasmas **18**, 062309 (2011).

[17]WANG, W., et al., Computer Physics Communications **164**, 178 (2004).

[18]KOLESNIKOV, R.A., et al., Phys. Plasmas **17**, 022506 (2010).

[19]KIM, J., et al., Phys. Rev. Lett **72**, 2199 (1994).

[20]BELL, R.E., et al., Phys. Rev. Lett **81**, 1429 (1998).

[21]BELL, R.E., et al., Phys. Plasmas **17**, 082507 (2010).

[22]FIELD, A., et al., Plasma Physics **51**, 105002 (2009).

[23]DIF-PRADALIER, G., et al., Phys. Rev. Lett **103**, 065002 (2009).

[24]WALTZ, R.E., et al., Phys. Plasmas **14**, 122507 (2007).

[25]WALTZ, R.E., et al., Phys. Plasmas **16**, 079902 (2009).

[26]KOLESNIKOV, R.A., Plasma Physics **52**, 1 (2010).

[27]BAYLOR, L., et al., Phys. Plasmas **11**, 3100 (2004).

[28]HAWRYLUK, R.J., *An empirical approach to tokamak transport* (Physics of Plasmas Close to Thermonuclear Conditions, 1980), vol 1, ed B. Coppi *et. al.*

[29]GOLDSTON, R., et al., Journal of Computational Physics **43**, 61 (1981).

[30]ST.JOHN, H.E., et al., *Plasma Physics and Controlled Nuclear Fusion Research, Seville,1994* (International Atomic Energy Agency, Vienna, Vol. 3 p. 603, 1995).

[31]CROMBÉ, K., et al., Phys. Rev. Lett **95**, 1 (2005).

**ACKNOWLEDGMENT**

This work supported in part by the U.S. Department of Energy under DE-FC02-04ER54698 and DE-AC02-09CH11466.